Applying Polymer Blend Dynamics Concepts to a Simplified Industrial System. A Combined Effort by Dielectric Spectroscopy and Neutron Scattering

Thomas Gambino,[*,†,‡] Angel Alegría,[*,¶,†] Arantxa Arbe,[†] Juan Colmenero,[¶,†,§] Nicolas Malicki,[‡] Séverin Dronet,[‡] Benoît Schnell,[‡] Wiebke Lohstroh,[‖] and Kirill Nemkovski[⊥]

†*Centro de Física de Materiales (CSIC, UPV/EHU) and Materials Physics Center MPC, Paseo Manuel de Lardizabal 5, E-20018 San Sebastián, Spain*

‡*Manufacture Française des Pneumatiques MICHELIN, Site de Ladoux, 23 place des Carmes Déchaux, F-63040, Clermont-Ferrand, Cedex 9, France*

¶*Departamento de Física de Materiales (UPV/EHU), Apartado 1072, E-20080 San Sebastián, Spain*

§*Donostia International Physics Center (DIPC), Paseo Manuel de Lardizabal 4, E-20018 San Sebastián, Spain*

‖*Heinz Maier-Leibnitz Zentrum, Technische Universität München, Lichtenbergstraße 1, D-85748 Garching, Germany*

⊥*Forschungszentrum Jülich GmbH, Jülich Centre for Neutron Science (JCNS) at Heinz Maier-Leibnitz Zentrum (MLZ), Lichtenbergstr. 1, 85748 Garching, Germany*

E-mail: gthomas001@ikasle.ehu.eus; angel.alegria@ehu.eus

Abstract

In this work we apply the methodology and concepts developed over the last years for the study of segmental dynamics on miscible polymer blends to the investigation of a blend made of styrene-butadiene rubber (SBR) and an oligomer of polystyrene (PS), as an example of simplified industrial system. In this way we obtain detailed information about the segmental dynamics of both components within the blend. To this end, a judicious combination of broad-band dielectric spectroscopy (BDS) and quasi-elastic neutron scattering (QENS) results on deuterium-labelled blends was required. Difficulties on the comparison between isotopically different samples arose due to changes in polymer microstructure associated with the obtention of deuterated polymers. Nevertheless, the strategy for data analysis developed in this work made it possible to readily resolve the components' segmental dynamics of the investigated mixtures. It was found that Gaussian distributions of the components' effective glass-transition temperatures provide a very good description of all the experimental data collected in the SBR/PS (50/50 wt%) mixtures over the whole accessible temperature range, not only by BDS and QENS but also those obtained by differential scanning calorimetry and by neutron elastic-fixed-window-scans experiments.

Introduction

Blending polymers is an efficient tool to obtain new materials with tailored properties.[1] Particularly, in tire industry blending is used in connection with the fine tuning of the glass-transition temperature T_g to modify mechanical properties of materials.[2] Regarding the application, the aim is to reduce the rolling resistance and increase the dissipation of energy during a braking period. These processes correspond to two distinct ranges in terms of frequency? (respectively 10-10^2 Hz and 10^4-10^7Hz). Therefore, the understanding of the dynamical behavior of the tire material in these frequency ranges is key in order to improve the mechanical properties of the rubber blend.

From a phenomenological point of view, it is well known that standard differential scanning calorimetric (DSC) measurements in a blend reveal a broad feature ranging almost between the two pure polymers' T_gs. From such a broad function, a concentration-dependent 'global' T_g of the blend is deduced. Nowadays it is well known that thermally activated concentration fluctuations have to play an important role in the observed broadening effect of the DSC traces; however, they are not the only decisive ingredient. In recent decades the complex dynamics in blends have been investigated in detail using canonical miscible blends as polystyrene/poly(vinyl methyl ether) (PS/PVME), polyisoprene/poly(vinyl ethylene) (PI/PVE) or poly(ethylene oxide)/poly(methyl methacrylate) (PEO/PMMA).[3,4] In those studies it was found that an effective T_g can be identified for *each* blend component,[5] which reflects the underlying dynamic heterogeneity[6–9] –i. e., the existence of two segmental dynamics, each of them associated to each of the two components. The presence of two effective glass-transitions in polymer blends was first attributed to the chain connectivity of each component,[10] although it has been shown that it is a more general phenomenon that occurs also in mixtures of smaller molecules.[11,12] A main idea behind this concept is that the relevant cooperativity size at the glass-transition could be comparable to the repeating unit (or molecular) size. Thus, in a volume around a given component c the fraction occupied by units of this same component is larger than the average ('macroscopic') concentration (ϕ^c),

giving rise to an effective concentration of this blend component ϕ^c_{eff} higher than the average one. This fact was captured with the concept of self-concentration (ϕ_s),[10] which allows connecting the effective and the macroscopic concentration as: $\phi^c_{eff} = \phi^c_s + (1-\phi^c_s)\phi^c$. In this way, the effective glass-transition of a given blend component in the blend can be defined as: $T^c_{g,eff} = T_g(\phi^c = \phi^c_{eff})$, where $T_g(\phi^c)$ refers to the above mentioned average-concentration dependent overall T_g determined e. g. from the broad DSC trace.

The above commented ideas show that the complex dynamical behavior of polymer blends mainly arise from the combination of two major ingredients: i) thermal fluctuations of concentration and ii) inherent dynamic heterogeneity between the blend components. The fundamental investigations on the segmental dynamics of polymer blends giving rise to this conceptual framework have been developed by using experimental techniques that can provide selectivity to the individual blend components, for instance dielectric spectroscopy (DS),[13] quasielastic neutron scattering (QENS),[14] and nuclear magnetic resonance (NMR),[15] among others. Specifically, broad-band dielectric spectroscopy (BDS) is a well-established tool to study polymer dynamics over a very broad frequency range.[13] However, only if the dielectric relaxation of one of the components is negligible the dynamics of the other component can be isolated. On the other hand, QENS combined with partial deuteration provides selective information about the hydrogen dynamics due to the much larger ($\approx \times 20$) neutron scattering cross-section of the hydrogen nucleus as compared to deuterium or any other kind of atom found in typical polymers.[14] The dynamic range covered by QENS is relatively narrow but it overlaps with that of BDS experiments at high frequencies. Moreover, QENS provides additional spatial information about hydrogen self-motions thanks to the dependence of the measured intensities upon the momentum transfer, Q, corresponding to the scattering events. Thus, the combination of BDS and QENS has been largely exploited to access the dynamics of polymer mixtures of different types as, athermal polymer blends, plasticized polymers, polymer nanocomposites, etc. [16]

The aim of this work is to apply the above described methodology to the investigation

of the dynamics of a simplified industrial system, particularly a blend of styrene-butadiene rubber (SBR) with an oligomer of polystyrene (PS), in order to obtain detailed information about the segmental dynamics of both components in the blend. Mixtures of these polymers are good candidates to simultaneously fulfill the desired reduction of rolling resistance and increase of energy dissipation during braking. Using PS-oligomers, the high-T_g component acts as a plasticizer. The entanglement network is not influenced, but varying the oligomer concentration allows tuning the average T_g of the system; also, miscibility is favored by using smaller macromolecules. In practice, it is observed that using these oligomers the greep performance is improved. On the other hand, from an academic point of view we note that it is not obvious *a priori* that theoretical frameworks developed and checked on canonical systems would also apply to the complex case of a mixture of a copolymer and an oligomer. As experimental techniques, we used DSC, BDS and neutron scattering (both, quasielastic as well as elastic fixed window scan measurements, together with diffraction with polarization analysis). To exploit neutron scattering selectivity, the use of samples where one of the components is deuterated is mandatory. The obtention of deuterated compounds yield changes in polymer microstructure posing difficulties in the joint analysis of the experimental results. They were overcome by the judicious combination of BDS and QENS results on all the partially deuterated samples used in this work, based on applying a model which considers both key ingredients in blend systems –dynamic heterogeneity and concentration fluctuations. The results obtained in this way show that the effect of blending PS oligomer with SBR on each component is mainly encoded into a distribution of effective T_gs originated from these combined ingredients. The temperature range covered by the obtained distributions nicely agrees with that of the broad glass-transition feature characterizing these materials as observed by DSC. Moreover, we also find a nice agreement between the deduced effective T_g-range of the individual components and the onset of the 'microscopic softening' revealed by the neutron elastic scans. Noteworthy, these good agreements are obtained despite the complexity of the investigated mixtures, where already the dynamical properties of the pure

components are noticeable affected by relatively small differences in copolymer composition and/or microstructure of the polymers involved. This gives support to the robustness of the approach followed. Conversely, the analysis of the Q-dependence of the QENS results reveals non-Gaussian effects that could be attributed to the inherent heterogeneous atomic motions of the components even in the high temperature range accessed by this technique –where the effects of the distributions due to concentration fluctuations are expected to be practically negligible.

Experimental

a. Samples.

Styrene-butadiene rubber (SBR) was obtained from Michelin laboratory.[17] d_8-Styrene and d_6-butadiene deuterated monomers were supplied by Cortecnet (purity of 99%) and Eurisotop (purity of 99%), respectively. Before their use for copolymerization, the monomers were first dried over BuLi for d_6-butadiene and over calcium hydride and dibutyl magnesium for d_8-styrene and then distilled to obtain purifed monomers. Similarly to hydrogenated SBR (hSBR) copolymers in classical runs, the deuterated SBR (dSBR) copolymer samples were synthesized by anionic polymerization by the Michelin Company. The copolymerization was initiated by BuLi in methylcyclohexane at 50°C. Deuterated monomers were mixed in appropriate conditions to adjust microstructures of the hydrogenated chains synthesized. The protonated polystyrene (hPS) and deuterated polystyrene (dPS) samples (purchased from Polymer Source) were synthesized by living anionic polymerisation of respectively styrene and styrene-d_8. Table 1 shows the microstructural composition, average molecular weight ($\overline{M}_n$) and polydispersity values ($\overline{M}_w/\overline{M}_n$) of the pure components used in this study. Blends (50% in weight) were prepared by solution casting using Tetrahydrofuran (THF) as a solvent. The obtained films were carefully dried under vacuum at 350 K for 24 h to remove the solvent completely. Reference samples of the neat polymers were prepared in a similar way.

Table 1: Sample characteristics obtained by size exclusion chromatography (SEC) using THF as an eluent. The 1,2-butadiene (vinyl), 1,4-butadiene and styrene contents are given in mass %.

Sample	1,2 butadiene	1,4 butadiene	styrene	$\overline{M}_n$ (kg/mol)	$\overline{M}_w/\overline{M}_n$
hSBR	33	47	20	22.8	1.03
dSBR	31	45	24	24.3	1.08
hPS	-	-	100	0.80	1.12
dPS	-	-	100	0.90	1.09

b. Differential Scanning Calorimetry.

Differential Scanning Calorimetry (DSC) measurements were carried out on approximately 10 mg of sample using a Q2000 TA Instrument. A helium flow rate of 25 mL/min was used throughout. Measurements were performed by placing the samples in sealed aluminum pans. Data were acquired during cooling at 3 K/min from 373 K to 173 K. Temperature-modulated experiments (TMDSC) were performed using a sinusoidal variation of 0.5 K amplitude and 60 s period.

c. Neutron Scattering.

The intensity recorded in a neutron scattering experiment contains coherent and incoherent contributions. The coherent part is related to relative positions of pairs of atoms and gives information about the structural organization and collective dynamics of the system while the incoherent contribution contains information about single atom dynamics. The incoherent cross-section of the hydrogen nucleus is overwhelming as compared to the cross-sections (both, coherent and incoherent) of carbon, oxygen and deuterium. Therefore, deuteration of a given component in the system leads to a huge suppression of the contribution of such a component to the scattered intensity. In this way, we can selectively follow the H-self motions of the remaining protonated component in our system. In this work we have followed this strategy. Thus, the samples investigated were blends of polymers where one of the components was protonated and the other one deuterated. We also studied the pure

protonated samples as reference. In order to determine the relative contribution of coherent and incoherent scattering to the measured cross sections, polarization analysis was used (see the Supplementary Information, SI). On the other hand, the dynamic information is provided by QENS measurements through the energy transfer ($\hbar\omega$) analysis of the scattered neutrons.

Time of Flight. The cold neutron Time-of-Flight (ToF) spectrometer TOFTOF at MLZ was used with an incident wavelength λ=7.0 Å, leading to an energy resolution $\delta\hbar\omega$ of 12.5 μeV (Half Width Half Maximum, HWHM). The acquired data were corrected for detector efficiency, sample container and absorption using the standard programs available at MLZ. The experimental scattering function $S_{exp}(Q,\omega)$ was finally obtained by constant-Q interpolation, reducing thus the effective Q-range to $0.6 \leq Q \leq 1.4$ Å^{-1}.

Backscattering. The backscattering QENS experiments were also carried at the MLZ, by means of the SPHERES instrument. The λ of the detected neutrons was set to 6.271 Å, resulting in an elastic energy resolution of nearly Gaussian shape ($\delta\hbar\omega = 0.5$ μeV, HWHM). The Q-range covered was between 0.2 and 1.8 Å^{-1}. Raw data were corrected for detector efficiency and sample container. In both QENS instruments, data were recorded at various temperatures above the T_gs of the samples, and the detector efficiency was determined from a standard vanadium sample. For deconvolution of the spectra, the instrumental resolution was determined by measuring the hSBR sample at 10 K (TOFTOF) and a fully protonated blend at 3 K (SPHERES). By means of SPHERES we also recorded Elastic Fixed Window Scans (EFWS) on the blends. In EFWS the recorded intensity only includes the elastic term $S_{el}(Q) = S_{exp}(Q, \omega \approx 0)$. Depending on the instrumental resolution, the EFWS intensities also contain quasi-elastic contributions with energy transfers smaller than the resolution of the spectrometer $\delta\hbar\omega$ (amplitude of the quasielastic signal at $\approx \delta\hbar\omega$). Data were recorded at the different detectors as function of temperature and subsequently normalized by their asymptotic low-T value.

Each sample was deposited between two aluminium foils and placed in a flat aluminium

container. The thicknesses of the samples were selected to provide a transmission higher than 90%, for which multiple scattering effects can be neglected.

d. Broad Band Dielectric Spectroscopy.

Broad-band Dielectric spectroscopy (BDS) experiments were conducted by using an Alpha dielectric analyzer (Novocontrol) to determine the complex dielectric permittivity ($\varepsilon^*(\omega) = \varepsilon'(\omega) - i\varepsilon''(\omega)$) over the frequency range $f = \omega/(2\pi)$ from 10^{-2} to 10^7 Hz. Samples were placed between two flat gold-plated electrodes (20 mm diameter) forming a parallel plate capacitor with a 0.1 mm thick cross-shaped spacer of Teflon of negligible area between them. The temperature was controlled by a nitrogen-jet stream with a Novocontrol Quatro temperature controller. Frequency sweeps were performed at constant temperature with a stability better than 0.05 K.

Results

a. Differential Scanning Calorimetry.

The calorimetric T_gs of the samples were determined using TMDSC by picking up the inflexion point of the reversible part of the heat flow (see Fig. 1). Starting with the neat systems, we note some differences in T_g between the protonated polymer and its respective deuterated counterpart for both SBR and PS, that could be attributed to the small differences in their microstructures, molecular masses and/or to isotopic effects (see Table 1). Due to their relatively low M_n, neat PS-oligomer samples show T_g-values around 280 K, significantly lower than the typical T_g value of PS. Even so, the values of T_g for the pure SBR samples are markedly lower –SBRs display their T_gs around 213 K (note that for the SBR investigated M_n(SBR) $\approx$ 23 kg/mol is much larger than the entanglement mass M_e(SBR) $\approx$ 3 kg/mol). The difference between the T_gs of the two pure components, ΔT_g, is thus close to 70 K and their blends can be considered as binary dynamically asymmetric blends.[4] In this case, SBR

is the low-T_g (fast) component and polystyrene the high-T_g (slow) component. As expected, the glass-transition processes of the blends manifest as broad features in the range between the T_gs of the pure components. Though nowadays it is established that each of the components display a different segmental relaxation in the blend, the corresponding effective T_gs are usually difficult to be resolved in the DSC traces. Therefore, to a first approximation, we have characterized the DSC results in the blends in the same way as in the homopolymers, namely by determining the inflection point. The such obtained results are listed in Fig. 1.

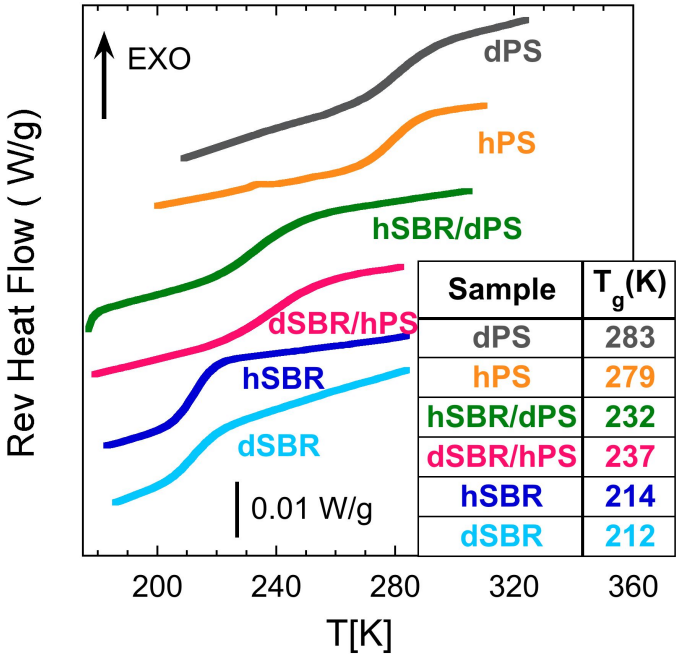

Figure 1: Reversible heat flow during cooling at 3 K/min for the samples investigated.

b. Elastic Fixed Window Scans.

With increasing temperature the increasing mobility of the scattering centers (protons) translates into a decrease of the elastic contribution to the neutron scattering spectra. From the Q-dependence of this intensity, the mean squared displacement of the scattering centers at a time determined by the instrumental resolution $\langle r^2_{t_{Res}}(T)\rangle$ ($t_{Res} \approx 1/\omega_R$, where $\hbar\omega_R = \delta\hbar\omega$) can be estimated as explained in the SI. In the case of SPHERES, t_{Res} is of the order of

the nanosecond. Because of being a magnitude which depends on the instrumental resolution, we will call it effective mean squared displacement. We also note that its determination is subjected to uncertainties due to several factors, in particular it can be affected by coherent contaminations (see SI). The values of $\langle r^2_{t_{Res}}(T)\rangle$ obtained for the two blends investigated are represented as function of temperature in Fig. 2.

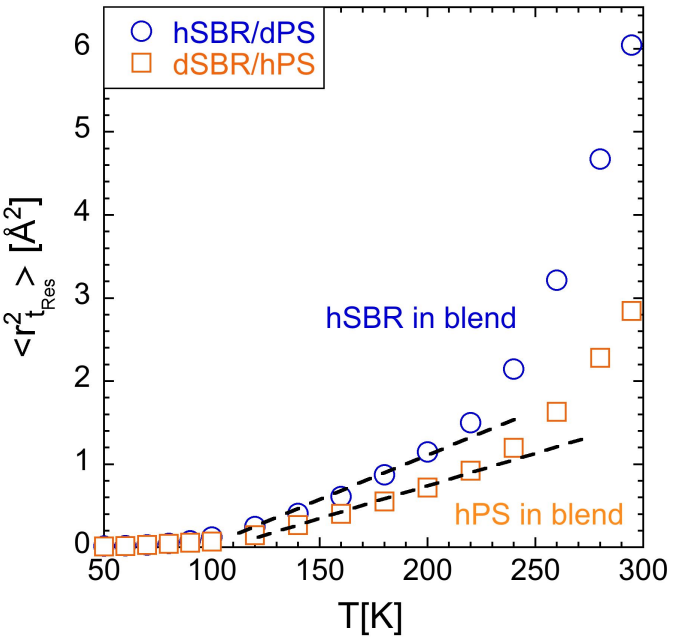

Figure 2: Temperature dependence of the effective mean squared displacement of protons obtained from fitting Eq. 2 (SI) in the two blends investigated. Dashed lines are guides to the eye displaying a linear increase in the intermediate temperature region.

As can be seen in Fig. 2, the spatial extent of the atomic motions shows a nearly linear increase at temperatures where we expect glassy behavior for the samples according to the DSC experiments. A more dramatic increase is found at higher temperatures, which could be attributed to the dynamics of the segmental relaxation. Though qualitatively similar, the results for both samples develop in a different way, namely in a more moderate fashion for the sample dSBR/hPS. We remind that for this sample the neutron scattering results reflect the motions of the protons of the hPS component in the dSBR/hPS blend, while for hSBR/dPS they correspond to the motions of the protons in the hSBR chains of the hSBR/dPS mixture. As can be observed in Fig. 2, for a given temperature, the molecular motions undergone by

the hSBR component in the blend lead to significantly larger hydrogen displacements than those active in the hPS component of the dSBR/hPS mixture.

c. Quasielastic Neutron Scattering.

SBR Dynamics

We first present the results on the homopolymer hSBR as a representative example for the data analysis, which will also serve as reference for the blend results. For a Q-value of 0.6 Å^{-1} Figure 3 shows respectively ToF (Fig 3(a)) and backscattering (Fig. 3(b)) spectra normalized to their maxima as a function of the energy transfer. The data are compared with the respective resolution function. For the conditions chosen, the spectra collected in both spectrometers display a clear quasielastic broadening, indicative for dynamical processes with characteristic times in the region of those accessible by the instruments (tens of picoseconds to nanoseconds). To analyze the data, the spectra $S_{exp}(Q,\omega)$ measured in the energy domain were Fourier transformed into the time domain, obtaining the –still affected by the resolution– experimental intermediate scattering function $S_{exp}(Q,t)$. We remind that a convolution product in the frequency domain translates into a simple product in the time domain. Thereby, the $S_{exp}(Q,t)$ functions were subsequently deconvoluted from the instrumental resolution by division by the corresponding Fourier transformed resolution signal, i.e., calculating $S(Q,t) = \frac{S_{exp}(Q,t)}{S_{res}(Q,t)}$. Figure 4 shows as an example the final intermediate scattering function obtained from the experimental data displayed in Fig. 3. Since different reference samples were used for determining the resolution of each instrument, the amplitudes of the resulting deconvoluted functions were affected by suitable matching factors. As can be appreciated in Fig. 4, with the wavelength used at TOFTOF, the Fourier time ranges of the two instruments almost overlap at about 0.1 ns and the degree of freedom for the adjustment of the amplitudes is very narrow. We also note that the combination of the results from TOFTOF and SPHERES allows covering over nearly 4 decades in the time domain.

By now it is well established that well above T_g, at local length scales of the order of the intermolecular distances (few Angstroms), the main dynamical process driving the atomic motions in glass-forming systems is the decaging process involved in the structural or α-relaxation.[18] In such a range, the intermediate scattering function describing this phenomenon can be approximated by a stretched exponential or Kohlraush-Williams-Watts functional form:[19]

$$S_{KWW}(Q,t) = A(Q)\exp\left[-\left(\frac{t}{\tau_{KWW}(Q)}\right)^{\beta(Q)}\right] \quad (1)$$

Here β is the stretching parameter describing the deviations from the exponential behavior ($0 < \beta \leq 1$, and close to 0.5 for most polymers)[20] and τ_{KWW} the characteristic relaxation time. The prefactor A determines the amplitude of the function and accounts for faster dynamic processes. As can be seen in Fig. 4, this functional form describes well the intermediate scattering function also in the samples here investigated.

Figure 5(a) shows the resulting relaxation times for hSBR. They follow well a power law

$$\tau_{KWW}(Q,T) = a(T)Q^{-b}. \quad (2)$$

The b-parameter is found to be close to 3.5 for all the temperatures investigated for hSBR. We note that for a pure diffusive behavior $b = 2$.[21,22]

Figure 5(b) presents the stretching parameter β as function of Q. We found $0.3 < \beta < 0.6$, with a tendency to decrease with increasing Q. Figure 6(a) shows the temperature dependence of the β-value averaged over the Q-range investigated, $\langle\beta\rangle$. The bars in this figure mark for each temperature the interval within which the β-values are found for the different Q-values investigated. A general tendency of the values of the shape parameter to increase with increasing temperature can be observed.

For anomalous ($\beta < 1$) diffusion-like behavior, if the Gaussian approximation is fulfilled the β- and b-values are connected to each other as: $\beta \cdot b = 2$.[23] In Fig. 6(b) the product of b and

the data displayed in Fig. 6(a) is represented. The values found are smaller than the Gaussian expectation, but tend to approach it at high temperatures. These results would be indicative of non-Gaussian effects usually interpreted in relation with dynamic heterogeneities.[4]

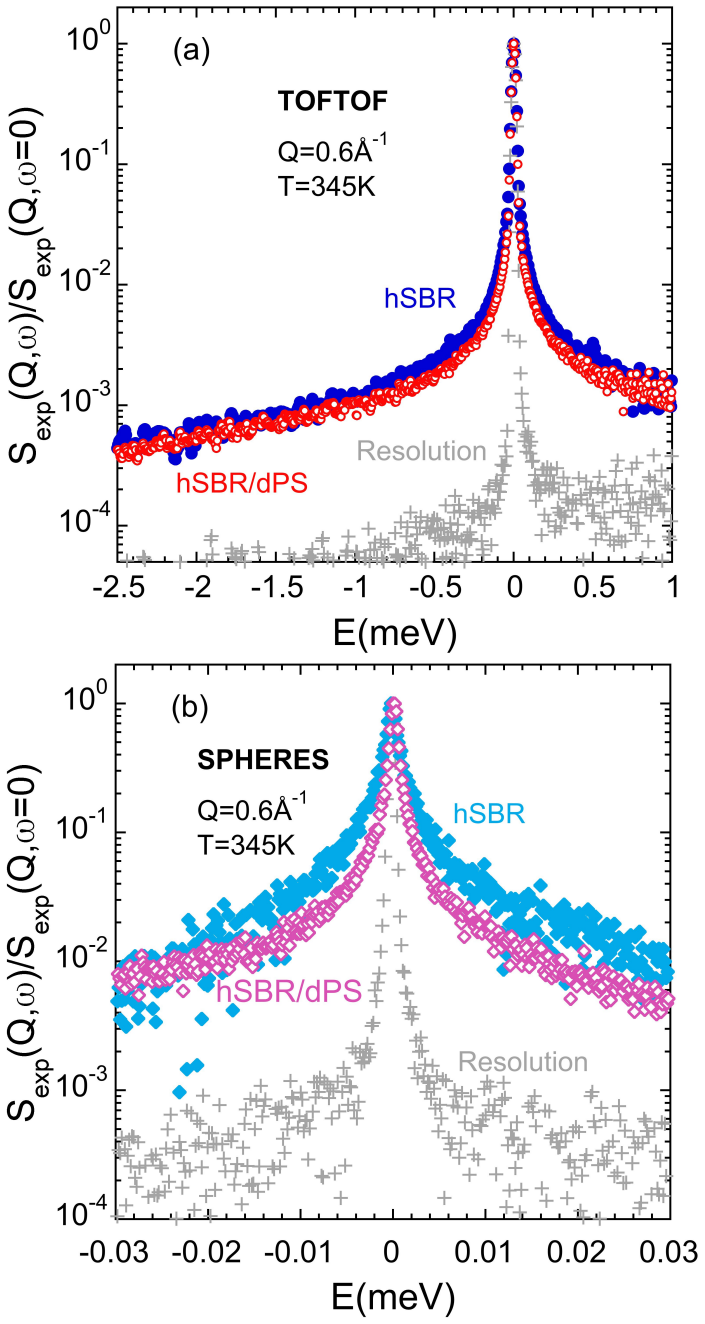

Figure 3: Normalized spectra measured by TOFTOF (a) and SPHERES (b) at $Q = 0.6$ Å^{-1} and $T = 345$ K compared with the corresponding resolution (crosses). Filled symbols correspond to the hSBR homopolymer and empty symbols to the hSBR/dPS blend.

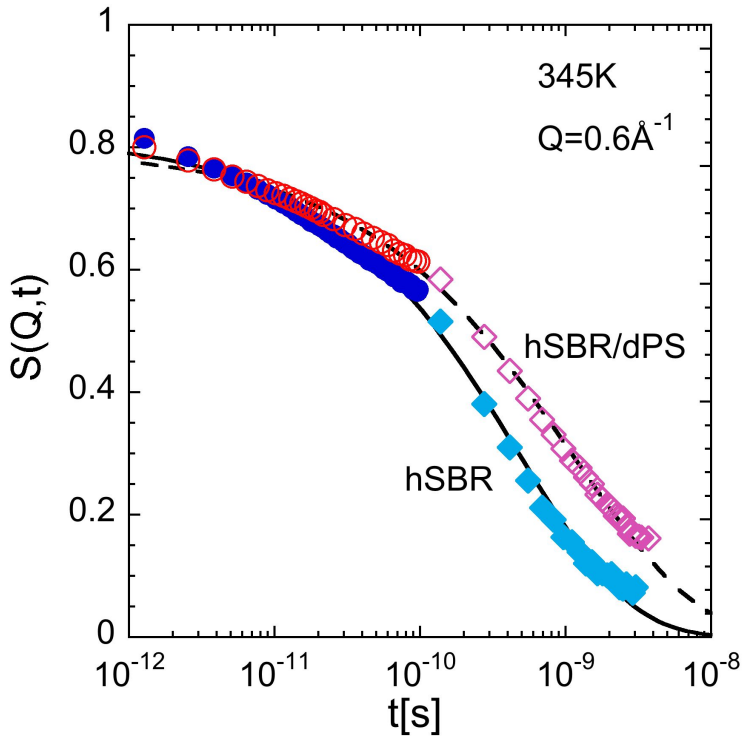

Figure 4: Intermediate scattering function obtained by Fourier transform and deconvolution of the results shown in Fig. 3 (same symbol code). Lines are fits of KWW functions (Eq. 1) to the experimental results for $t \geq 2ps$.

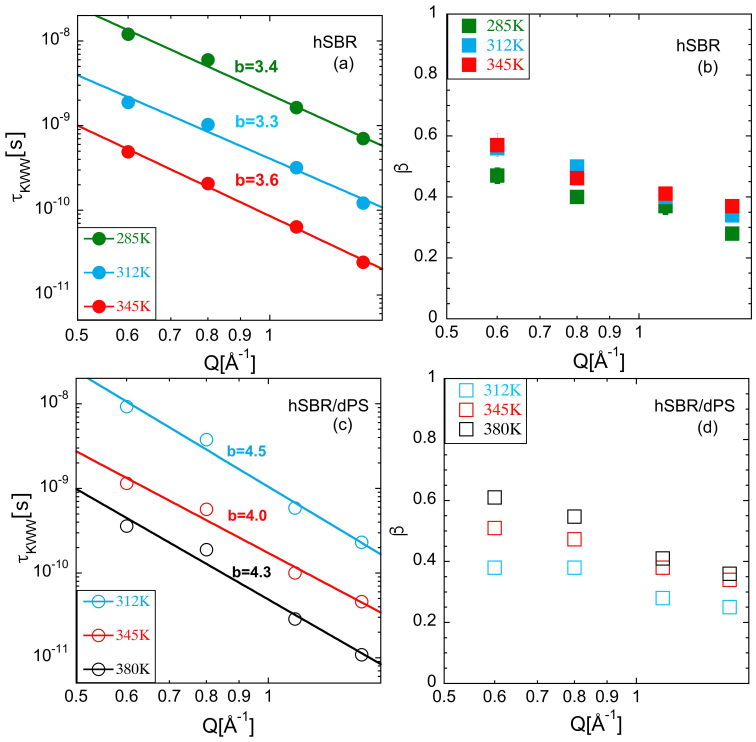

Figure 5: Momentum transfer dependence of the characteristic times (a, c) and stretching exponents (b, d) obtained from the KWW fit to the QENS results of hSBR (a, b) and the blend hSBR/dPS (c, d) at the different temperatures investigated. Lines are fits of Eq. 2 with the b-values indicated.

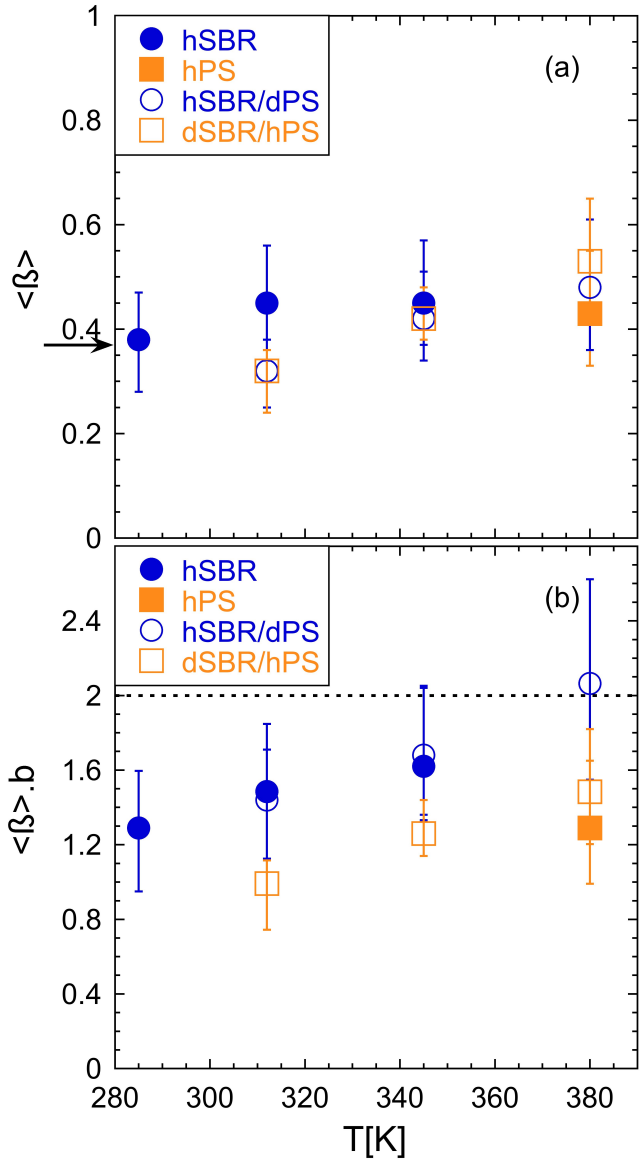

Figure 6: Temperature dependence of (a) the value of the stretching parameter averaged over the Q-range investigated and (b) the product of this average and the parameter determining the power-law dependence of the characteristic times obtained from the KWW-fits of the QENS data for the different samples investigated. The bars mark the interval within which the β-values (respectively, the product $\beta \cdot b$) are found for the different Qs investigated. The arrow in (a) marks the β-value used to describe the dielectric results, and the horizontal dotted line in (b), the value in the Gaussian case.

We now present the results obtained for the dynamics of hSBR in the blend hSBR/dPS. The neutron intensity scattered by this sample at $Q \geq 0.5$ Å^{-1} is largely dominated by the incoherent scattering of the SBR hydrogens, as demonstrated by the DNS investigation (see SI). Figures 3 and 4 show that for hSBR in the blend, the QENS curves are narrower and correspondingly the intermediate scattering function decays at longer times than for hSBR in the homopolymer.

In the temperature and Q ranges here explored, the intermediate scattering function of the blend can be well described by KWW functions (see Fig. 4 as a representative example). Figure 5(c) shows the characteristic times obtained from the KWW fits, confirming a slowing down of the hSBR dynamics upon blending (compare Figs. 5(c) and (a)). The b-parameter values obtained from Eq. 2 for hSBR in the blend are close to 4.3 in average, i. e., higher than for pure hSBR ($b \approx 3.5$).

Figure 5(d) shows that the stretching parameter β for the hSBR/dPS slightly decreases when Q increases. The values, $0.25 < \beta < 0.6$, are in the same range as those obtained for hSBR, but change more with temperature. In particular, we observe significantly smaller β-values at 312 K for the blend than for the homopolymer. This can be better appreciated in Fig. 6(a). Figure 6(b) shows that the deviations from Gaussian behavior of the protons in hSBR are rather similar in the homopolymer and in the blend.

PS Dynamics

Figure 7(a) shows the relaxation times obtained from fitting the intermediate scattering function results for the pure sample, hPS, at the temeprature investigated of 380 K. Again they follow well a power law (Eq. 2) with $b = 3$. Figure 7(b) shows that for hPS β slightly decreases when Q increases. The product $\beta \cdot b$ for hPS also reveals non-Gaussian behavior, as can be appreciated in Fig. 6(b).

The dynamics of polystyrene in the blend was followed by the QENS experiments on the sample dSBR/hPS, which above $Q \approx 0.5$ Å^{-1} are largely dominated by the incoherent contribution from protons of the polystyrene component (see SI). The obtained characteristic

times reflect a faster dynamics for hPS in the blend as compared to the pure polystyrene, at a given Q and temperature (see Figs. 7(c) and (a)). Solid lines in Fig. 7(c) stand for the fit to Eq. 2. In average, the b-values are found to be rather close to 3, i. e., to that in pure hPS. The stretching parameter values deduced for the dSBR/hPS sample are plotted in Fig. 7(d) and their averages in Fig. 6(a). They show basically the same features as those determined for the hSBR component in the blend hSBR/dPS. However, in the respective blends the deviations from Gaussian behavior for the hPS component are markedly stronger than for the hSBR component.

In the phenomenological KWW description applied in this work there is no attempt to distinguish the origin of the possible different mechanisms for H-dynamics. One could however wonder about the importance of the translational diffusion component in the case of the PS oligomers. The estimations presented in the SI show that such contribution should not be of major relevance in the investigated dynamic window for the temperatures here explored.

d. Dielectric Spectroscopy.

Figure 8 shows representative examples of the frequency dependence of the dielectric loss peak $\varepsilon''(\omega)$ obtained at different temperatures for the pure polymers and the blends investigated by QENS. We observe a main loss peak attributable to the segmental dynamics (α-relaxation), which position strongly depends on temperature. In agreement with the DSC results, the dielectric peaks of the two homopolymers are centered at similar frequencies at much lower temperatures for SBR than for PS. From the peak values of the dielectric permittivity losses in Fig. 8, it can also be seen that SBR has a stronger dielectric relaxation than PS. By comparing the results on the mixtures with those on the homopolymers (Fig. 8(a) and (b)) it is apparent that the dielectric response of the blends is broader and intermediate between those of the neat systems, as already reported for other polymer mixtures (see,

e. g.[24] and[4] as general references). We also note that the BDS results of the two blends investigated by QENS, hSBR/dPS and dSBR/hPS, do not coincide for the same temperature. For example, at 255 K, the peak observed for the sample where the SBR component is protonated (hSBR/dPS, Fig. 8(a)) is centered at clearly higher frequencies than that displayed by the blend with the inverse isotopic label (Fig. 8(b)). Nevertheless, as an example, in the normalized representation $[\varepsilon''(\omega)/\varepsilon''_{max}]$ shown in Fig. 9, the hSBR/dPS results at 255 K look very much the same as those corresponding to the dSBR/hPS sample at 263 K. Since dielectric spectroscopy is not sensitive to deuteration, this temperature difference has to be attributed to the somewhat different microstructure of the blend components and/or to isotopic effects leading to distinct dynamics, as reflected in the DSC measurements. We note that clear differences are also visible in the dielectric relaxation between the deuterated and the protonated pure polymers, as it is illustrated in the SI.

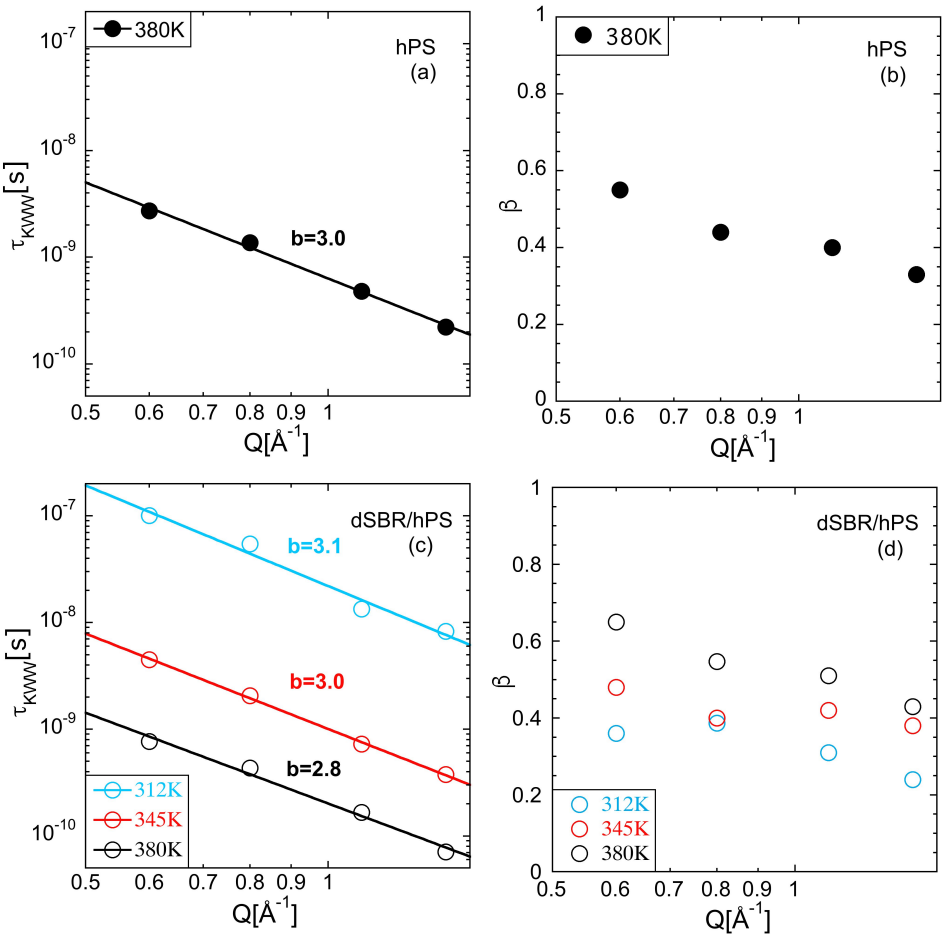

Figure 7: Momentum transfer dependence of the characteristic times (a, c) and stretching exponents (b, d) obtained from the KWW fit to the QENS results of hPS (a, b) and the blend dSBR/hPS (c, d) at the different temperatures investigated. Lines are fits of Eq. 2 with the *b*-values indicated.

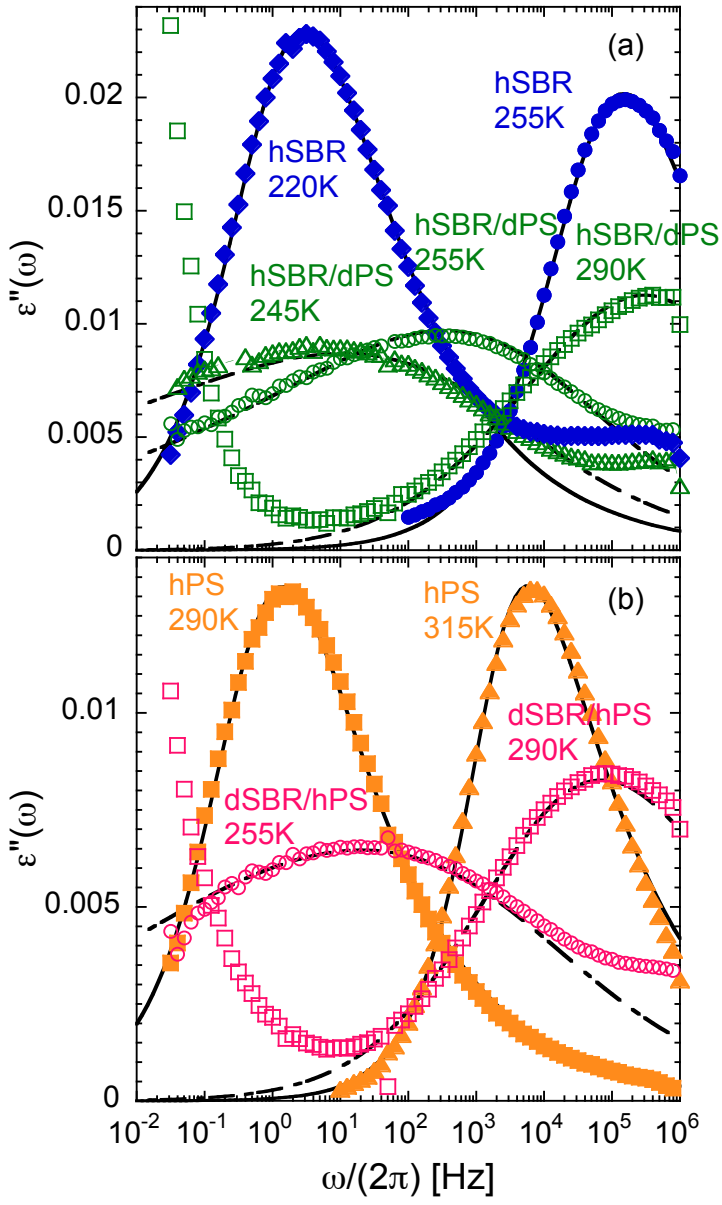

Figure 8: (a) Frequency dependence of the dielectric loss at 220 and 255 K for hSBR and for the blend hSBR/dPS at 245, 255 and 290 K. (b) Frequency dependence of the dielectric loss at 290 K and 315 K for hPS and for the blend dSBR/hPS at 255 and 290 K. In both panels, the solid lines stand for the fit of the pure polymers results (filled symbols) by means of the Havriliak-Negami equation (Eq. 4) and the dashed-dotted lines for the fit of the blends data (empty symbols) by means of the model proposed (see the text).

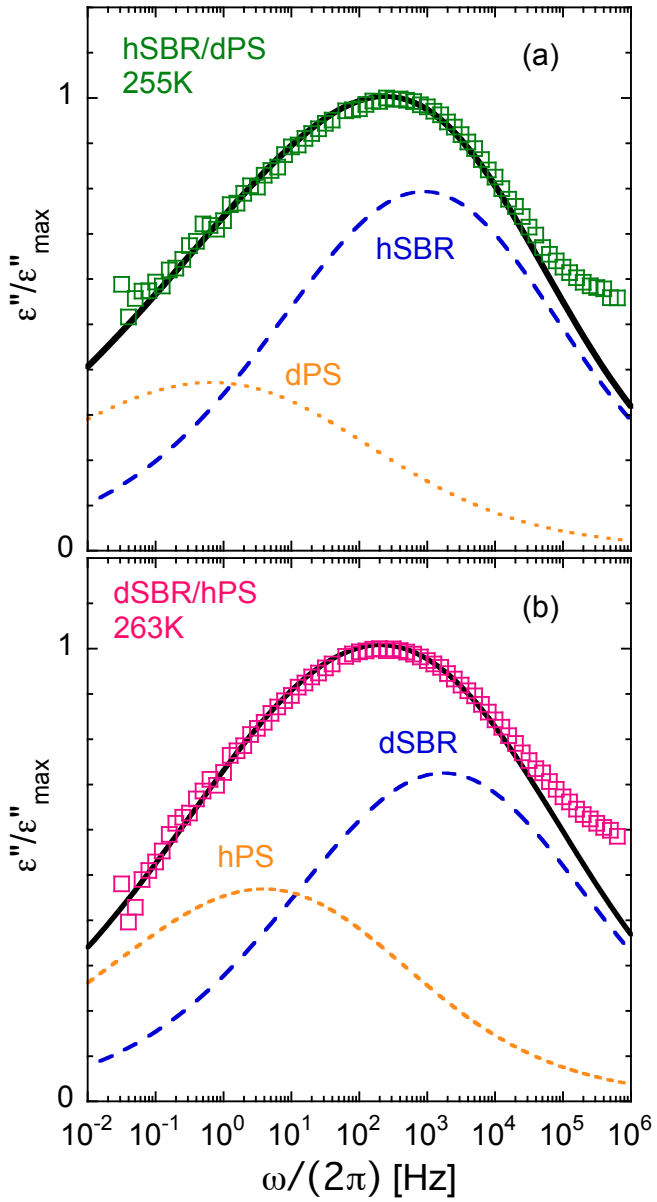

Figure 9: Normalized imaginary part of the dielectric permittivity for hSBR/dPS at 255 K (a) and dSBR/hPS at 263 K (b) as function of frequency. Solid lines stand for the fit by means of the proposed model. The contribution of each blend component is shown as dashed (SBR) and dotted (PS) lines.

Figure 10 shows the temperature dependence of the characteristic time scales, defined as the inverse of the angular frequencies at the dielectric loss maxima ($\tau_{max} = \omega_{max}^{-1}$) of the α-relaxation process for the pure polymers and the two blend samples investigated by QENS. For completeness, we have also included the results obtained on the deuterated homopolymers dPS and dSBR. The lines correspond to descriptions by means of the Vogel-Fulcher-Tammann VFT equation:[25–27]

$$\tau(T) = \tau_0 \exp\left[\frac{DT_0}{T - T_0}\right] \tag{3}$$

In the fits, we kept constant the prefactor value $\tau_0 \equiv 10^{-13}$ s in the VFT equation (Eq. 3). First, the data of the two protonated homopolymers were considered. The values obtained for the fragility parameter D and the Vogel temperature T_0 are displayed in Table 2. Fixing the D-value to that obtained for the protonated counterpart, the VFT function also describes very well the data on the deuterated homopolymers. In Table 2 we can see that the values of the Vogel temperatures differ upon deuteration reflecting the differences found by the DSC experiments. Conversely, considering that the blend dielectric results are partially dominated by the SBR component, for describing the blend data the value of the D-parameter was fixed to be the same as that determined from the fit of the hSBR results. As can be appreciated in Fig. 10, the quality of the descriptions is very good for both blend samples. The difference is a shift in the Vogel temperature of about 5 K.

Regarding the shape of the relaxation curves, as usual, the results on the pure polymers can be well fitted by means of the Havriliak-Negami (HN) equation[13] (see Fig. 8)

$$\varepsilon''_{HN}(\omega) = -Im\left\{\frac{\Delta\varepsilon}{[1 + (i\omega\tau_{HN})^{\alpha}]^{\gamma}}\right\} \tag{4}$$

where $\Delta\varepsilon$ is the dielectric relaxation strength, τ_{HN} is the characteristic relaxation time, and the fractional shape parameters α and γ describe respectively the symmetric and asymmetric broadening of the complex dielectric function $0 < \alpha;\ \alpha \cdot \gamma \leq 1$ holds. Despite the fact

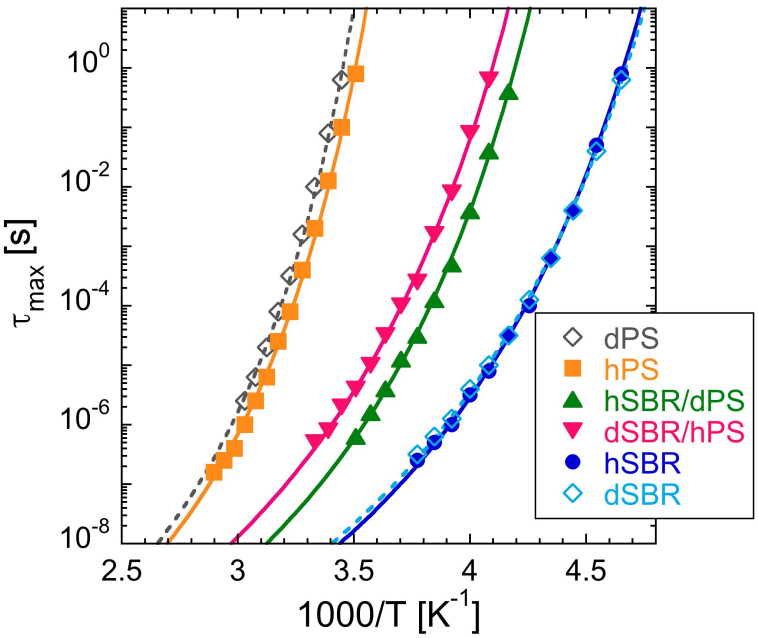

Figure 10: Temperature dependence of the characteristic times defined from the inverse of the frequencies of the dielectric loss maxima for the α-relaxation process of the different samples investigated. The lines correspond to descriptions by means of the VFT equation with $\tau_0 \equiv 10^{-13}$s. Empty symbols (corresponding fitting curves as dotted lines) stand for the deuterated homopolymers.

that the low frequency part of the loss peaks of the homopolymers slightly narrows by increasing temperature, it was possible to obtain good descriptions of the experimental data in the whole temperature range investigated keeping the product $\alpha \cdot \gamma$ constant (see Fig. 8). Table 2 presents the parameter values used to describe the loss curves of the homopolymers at temperatures where the corresponding loss peak was well centered in the experimental frequency range (see representative examples in the SI). The extra losses observed at higher frequencies for SBR (see Fig. 8(a)) are originated by the contribution of the β-process. This is mainly due to local dynamics within cis 1,4-butadiene segments,[28,29] which was not included in the model function. We note that (under certain constraints) HN functions are descriptions of the Laplace transform of KWW relaxation functions.[30] The β-parameter value of the KWW function in the time domain corresponding to the HN functions describing BDS data can be calculated as $\beta \approx (\alpha \cdot \gamma)^{0.813}$ (see SI), which provides $\beta \approx 0.37$ for the

Table 2: Parameters involved in the VFT description of the characteristic times shown in Fig. 10 with $\tau_0 \equiv 10^{-13}$ s. For the homopolymers, the dielectric strength and Havriliak-Negami parameters obtained fitting the curves well centered in the experimental frequency window are also given, as well as the value of the characteristic time at the calorimetric glass-transition temperature, τ_g.

Sample	T_0[K]	D	$\Delta\varepsilon$	α	γ	τ_g[s]
hSBR	166.6	8.6	0.11	0.61	0.49	1.4
dSBR	166.4	8.6	0.09	0.47	0.63	3.0
hPS	231.7	6.9	0.06	0.70	0.43	47
dPS	235.3	6.9	0.06	0.65	0.46	74
hSBR/dPS	184.7	8.6	-	-	-	-
dSBR/hPS	190.1	8.6	-	-	-	-

investigated homopolymers.

The HN function does not describe well the blend data since extra contributions at low frequency are evident in the loss peaks. This feature is commonly found in polymeric mixtures[3] and occurs in the the blends investigated here not only because of the expected polystyrene contribution at frequencies significantly lower than the peak of SBR but also due to the presence of thermal concentration fluctuations.[31]

We now compare dielectric with QENS results. For both homopolymers, the stretching exponent β corresponding to the dielectric relaxation is in the range of the values obtained by QENS (see arrow in Fig. 6(a)). To compare the relaxation times, we have to take into account the Q-dependence of the time scale of the α-relaxation as measured by neutron scattering. In order to compare the dielectric and neutron scattering data we have first converted the QENS KWW time into a characteristic relaxation time corresponding to the maximum of the peak of the neutron dynamic susceptibility (τ_{max}). In principle, it is always possible to find a Q-value (we will call it $Q^\star$) at which the characteristic times of the α-relaxation determined by QENS become similar to those measured by BDS. As can be observed in Fig. 11(a), there is a good agreement between the VFT prediction of the high temperature dielectric data of hSBR and the values deduced by means of neutron scattering at $Q^\star_{SBR}$= 0.7 Å^{-1}.

Comparing the VFT line of hPS with the neutron data at 380 K, we find that $Q^\star_{PS}$= 0.55 Å^{-1}

(see Fig. 11(b)). Details of the transformation from τ_{KWW} to τ_{max} and the comparison between neutron and dielectric data are presented in the SI.

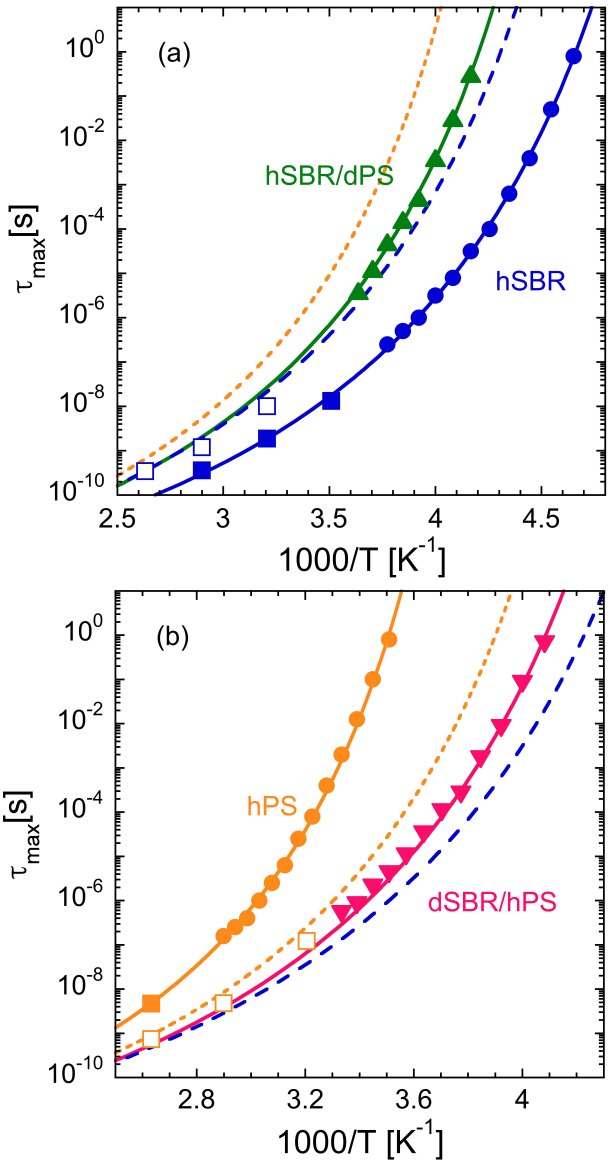

Figure 11: Temperature dependence of the characteristic times defined from the inverse of the frequencies of the loss maxima for the α-relaxation process obtained from dielectric spectroscopy (circles and triangles) and QENS at $Q^{\star}$ (squares). The solid lines correspond to a description of the dielectric data by means of the VFT equation. Dashed and dotted lines stand for the dynamics of the components in the blend (SBR and PS respectively, see text). Panel (a) shows the results for hSBR and the blend hSBR/dPS and panel (b) for hPS and the blend dSBR/hPS.

If we now consider the dynamics of hSBR in the mixture, we find that the QENS data on the blend hSBR/dPS at $Q^{\star}_{SBR}$= 0.7 Å^{-1} denote a slightly faster dynamics than the extrapolated high temperature dielectric data on the same sample (see Fig. 11(a)). This difference is what could be expected due to the non-negligible slow polystyrene contribution to the BDS results of the blend. Moving to the QENS results from the dSBR/hPS sample corresponding to hPS dynamics in the blend, the values of the characteristic times at $Q^{\star}_{PS}$= 0.55 Å^{-1} are slightly larger than those deduced from BDS on the same sample (see Fig. 11(b)). This observation could again be attributed to the fact that hPS in the blend is moving more slowly than the average, whereas the SBR component –dominating the $\varepsilon''(\omega)$ peak position– is faster than average.

Discussion

The experimental results on our blends show clear indications of dynamic heterogeneity at the segmental level. For instance, the EFWS results reveal markedly different motional amplitudes of the two components in the two blends investigated. Also, if the QENS results on the characteristic times of the polymer components are directly compared (see SI), a clearly faster dynamics can be found for hSBR in the hSBR/dPS blend than for the hPS component in the dSBR/hPS blend. This difference increases with decreasing temperature. We note however that a quantitative comparison of these results is not so straightforward, since there are differences in the dynamics of the neat components, as it has been mentioned above.

Another hint for dynamic heterogeneities in the blends can be found from the comparison between dielectric and DSC results. If, as a first approximation, we consider that the dielectric loss peak frequency in the blend mainly reflects the SBR-component dynamics, the fact that the fragility remains essentially unaltered for this component upon blending suggests that the change in T_g is the major reason for the changes in the SBR segmental dy-

namics in the blend. However, we note that the difference in the calorimetric glass-transition between the hSBR and the hSBR/dPS samples is 23 K, whereas the shift observed in the VFT temperature determined by BDS –attributable, in a first approximation, to the SBR component– is only 18 K. This difference is consistent with distinct segmental dynamics for the blend components, resulting in distinct effective glass-transition temperatures. In such a framework, ${T_g}^{DSC}$ is an average value of the T_gs of the blend components, as anticipated in the previous section. We may examine the DSC results in more detail in order to extract information about the different behavior of the two blend components.

The calorimetric glass-transitions of the studied blends are slightly asymmetric and very broad, extending over a T-range larger than 50 K for both blends. The temperature derivative of the reversible heat flow provides a sensitive way to detect glass-transition processes. Figure 12 shows this function for the blends and respective homopolymers. Two overlapping glass-transition ranges could be envisaged in the blends from the high temperature shoulder of the signals; however, a reliable determination of the effective glass-transition values corresponding to each component is not possible from the DSC results. This has been realized in some specific blends of polymers whose neat components differ by more than 100 K in their respective T_g values.[4,8,32]

In the following, we present a joint analysis of BDS and QENS results based on concepts previously developed and by now well established for model polymer blends. The specific information provided by neutron scattering on the protonated blend component will be a key ingredient to disentangle the component dynamics of the two kinds of polymers *in the same blend*.

As can be seen in Table 2, the predominant contribution to the dielectric response is that of the SBR component. However, the dielectric signal of PS is significant and there would be an underlying two-peak structure in the BDS spectra with contributions from the two kinds of polymeric chains. In order to identify the component contributions to the dielectric relaxation in the blends we have assumed that each of the two components contributes pro-

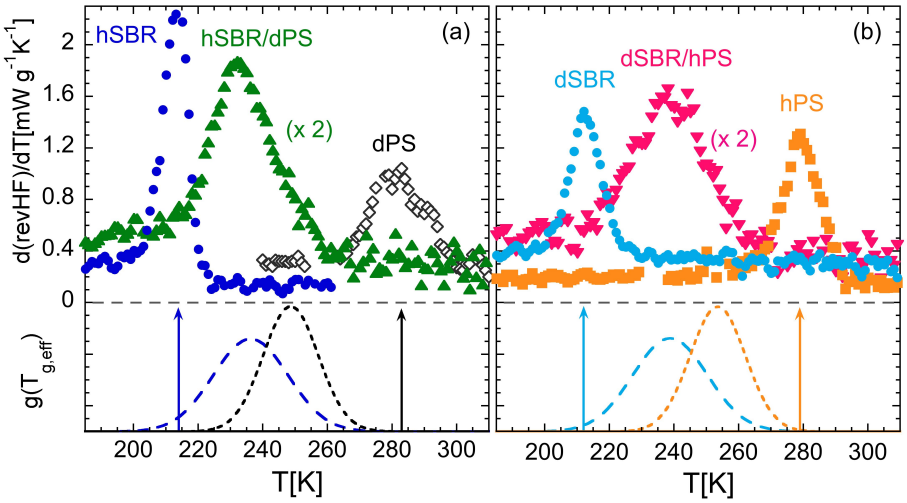

Figure 12: Derivative of the reversible heat flow for the blend hSBR/dPS (a) and dSBR/hPS (b) as function of temperature compared with that determined for the pure homopolymers. In the lower part of the figures, the arrows indicate the glass-transition temperatures of the neat polymers and the dashed (dotted) curves, the distribution functions of effective glass-transition temperatures of the SBR (PS) component deduced from the joint analysis of the QENS and BDS results.

portionally to the BDS signal measured in the corresponding pure polymer. In addition, we have assumed that the contribution of each component in the blend arises as a superposition of contributions similar in shape to those of the corresponding pure polymer, but with different relaxation times. This relaxation time distribution would be mainly attributed to the presence of concentration fluctuations.[31] As aforementioned, concentration fluctuations constitute the ingredient which, together with the self-concentration effects, are believed to be decisive in determining polymer blend dynamics. Following previous results,[24] it has been assumed that the effect of concentration fluctuations translates into a distribution of VFT temperatures $h(T_0)$ –equivalently, of effective glass-transition temperatures– for each of the components in the blend. The observed distributions of characteristic times are thus a conse-

quence of the spread of VFT-temperatures in the blend, since it is usually safely assumed that the other parameters in the VFT equation (D and τ_0) can be considered nearly insensitive to concentration.[33] For the SBR components we assumed the D and τ_0 values determined above by fitting the whole peak position, i.e. $\tau_0 = 10^{-13}$ s and $D^{hSBR} = D^{dSBR} = 8.6$. In the case of the PS components we fixed $\tau_0 = 10^{-13}$ s but not the value of the fragility parameter (assuming that $D^{hPS} = D^{dPS}$), since it is well documented that the fragility of the high-temperature component in polymer mixtures is actually reduced by blending.[7,33]

Under these assumptions, the dielectric loss peak of the blend would be expressed as:

$$\varepsilon''_{blend}(\omega) \propto \sum_c \phi_c \int \varepsilon''^{c}_{HN}(\omega, T_o) h^c(T_0) dT_0 \tag{5}$$

where the index c refers to the component of the blend (c: hSBR and dPS for the hSBR/dPS sample, c: dSBR and hPS for the dSBR/hPS sample). The concentration ϕ^c of each component is always 50 wt% in the samples here investigated. Each contribution to the component permittivity $\varepsilon''^{c}_{HN}(\omega, T_o)$ is taken with shape parameters as those determined from the fits of the corresponding homopolymer data (see Table 2). The dielectric relaxation strength of each polymer component in the blend is assumed to be half of that determined as the average value in the corresponding homopolymer (see Table 2). Finally, the distribution functions $h^c(T_0)$ are assumed to be Gaussian functions given by:

$$h^c(T_0) = \frac{1}{\sqrt{2\pi}\sigma_0^c} \exp\left[-\left(\frac{T_0 - \langle T_0^c \rangle}{\sqrt{2}\sigma_0^c}\right)^2\right]. \tag{6}$$

In this approach, the fitting parameters are the average value of the VFT-temperature $\langle T_0^c \rangle$ and the variance of the distribution σ_0^c for each component and one common fragility parameter D^{PS} (independent of isotopic substitution) . The fitting procedure consisted of three steps: In a first step, we determined the value of D^{PS}. To do this, we made use of the selective information provided by the NS results on the dSBR/hPS sample, that reveal the temperature dependence of the hPS component in this sample at high temperature. This

information however is not enough to univocally determine the value of the fragility for this blend component. Therefore, we tried to complement these high-temperature results with information from dielectric spectroscopy. We thus fitted the model function to the dielectric data of the same blend dSBR/hPS at 263 K, where the signal is well centered in the BDS window (see Fig. 9(b)). Assuming as first approximation the 'macroscopic' value, $D = 8.6$ for both blend components, we deduced an approximate value of the characteristic time of the PS-component in the blend at 263 K. The fit of a VFT function using this point value together with the high-temperature QENS data at $Q^\star$ allowed to determine the value of $D^{PS} = 7.6$ as the fragility of the PS component. A second step consisted of obtaining an estimation of the values of the parameters characterizing the distributions $h^c(T_0)$ for the two blends. This was realized on the selected BDS data shown in Fig. 9 where the loss peaks are well centered in the experimental window. Starting from the resulting estimated values, in the third step we applied the model to other temperatures, refining the values of the parameters $\langle T_0^c \rangle$ and σ_0^c. The final values are compiled in Table 3. The model provides a rather satisfactory description of the data, as can be appreciated in Figs. 8 and 9. The deviations at lower and higher frequencies are respectively due to conductivity and the above-mentioned β-relaxation contributions, both of which are not considered in the model function.

Table 3: Parameters describing the fragility and the distribution function of VFT temperatures of each component in the blends. The corresponding values of the distributions of effective glass-transition temperatures are also included (see text)

Component c	D^c	$\langle T_0^c \rangle$[K]	σ_0^c[K]	$\langle T_{g,eff}^c \rangle$[K]	σ_g^c[K]
hSBR in hSBR/dPS	8.6	184.0	9.0	236.3	11.6
dPS in hSBR/dPS	7.6	203.5	7.0	248.7	8.6
dSBR in dSBR/hPS	8.6	187.0	9.0	238.8	11.5
hPS in dSBR/hPS	7.6	207.0	7.0	253.6	8.6

The average T_0-values of the two components differ in about 20 K for both blends, translating in a clear dynamic heterogeneity in the mixture. From the above approach the resolved contributions of both components in the blends can be obtained, as shown in Fig. 9 (dashed and dotted lines). The resulting temperature dependence of the peak

relaxation times of the SBR and PS components in each blend is included in Fig. 11 as dashed and dotted lines respectively. The dynamic heterogeneity is patent when these peak characteristic times are resolved, leading to vitrification at different temperatures for each of the components, i. e., different effective glass transitions. Conversely, the influence of concentration fluctuations is mainly reflected in the width of the T_0-distribution, which is slightly larger for SBR compared with PS (see Table 3).

As commented above, the underlying distributions of VFT-temperatures also naturally imply distributions of the effective glass-transition temperatures of the blend components $g^c(T_{g,eff})$ given by $g^c(T_{g,eff}) = h^c(T_0)\frac{dT_0}{dT_{g,eff}}$. To obtain these functions, a connection between the VFT temperature and the glass-transition temperature has to be invoked. Since the value of the VFT temperature determines the characteristic time, what is needed is to establish the value of the characteristic time of the α-relaxation at the glass-transition temperature $\tau_g = \tau(T_g)$. Often, this time has been assumed to be $\tau_g \equiv 100$ s.[34] However, this value changes from sample to sample, and also depends on the technique and the criterion used for determining T_g.[35] For instance, for pure hSBR and hPS we found that the relationship between the dielectric α-relaxation time and the calorimetric T_g (defined as the inflection point in the DSC traces) is: $\tau_g^{hSBR}(T_g) = 1.4$ s and $\tau_g^{hPS}(T_g) = 47$ s (see Table 2). One possible approach is to assume that in the blend these relationships still hold. Then, the distribution of effective glass-transition temperatures can be easily calculated:

$$g^c(T_{g,eff}) = \frac{\ln(\tau_g^c/\tau_0)}{D^c + \ln(\tau_g^c/\tau_0)} h^c(T_0) \tag{7}$$

Since the $h^c(T_o)$ functions are assumed to be Gaussian, $g^c(T_{g,eff})$ are also Gaussian functions, with the values of the average $\langle T_{g,eff}^c \rangle$ and variance σ_g^c given by $\langle T_0^c \rangle [D + \ln(\tau_g^c/\tau_0)]/\ln(\tau_g^c/\tau_0)$ and $\sigma_0^c[D + \ln(\tau_g^c/\tau_0)]/\ln(\tau_g^c/\tau_0)$ respectively (see Table 3). These $g^c(T_{g,eff})$ functions are broader than the corresponding $h^c(T_0)$ ones, and their average values are separated by $\approx$ 12 K for the hSBR/dPS blend components and by $\approx$ 15 K for the hSBR/dPS blend com-

ponents. They have been represented in the lower parts of Figs. 12(a) and (b). We note that the simple addition of the distributions is not expected to reproduce the observed derivative of the heat flow; nevertheless, this comparison is very instructive to show the robustness of our approach and the good agreement between its results and independent measurements from different techniques: as can be seen, the calculated distributions span over the entire range where the experimental DSC signals of the blends reflect glass-transition phenomena.

Now we consider the selective microscopic information on proton motions provided by the neutron scattering experiments. In Fig. 2 we see that, at a given temperature, the effective mean squared displacement of the SBR protons is significantly larger than that of the PS protons. The increase of the atomic displacements is due to both, vibrational motions and dynamics associated to molecular mobility at different levels (rotations of side groups, localized motions involved in the secondary relaxations, the structural relaxation, and overall chain dynamics). Depending on the temperature, some of these processes are either completely frozen or, at least, slow enough to lead to contributions resolvable by the QENS instrument. Vibrations are naturally active at all the temperatures and are in fact the source of the small increase of the effective mean squared displacements observed below 100 K. The increase of the slope in this temperature range has to be attributed to the onset of localized motions of small portions of the chains including atoms at the main-chains and/or in the phenyl rings in the glassy state, as those responsible for the secondary relaxations detected by other techniques. In the glassy state, a larger mobility is expected for the atoms located at butadiene units than for those at the styrene monomers. As it has been mentioned above, the dielectric signal of SBR contains a β-process that reflects the local motions involved in the cis 1,4-butadiene component of this polymer. These motions obviously contribute to the increase of the proton mean square displacement monitored by the EFWS experiments. Regarding PS, QENS investigations[36] on the glassy dynamics of this polymer revealed small amplitude oscillations of increasing amplitude with temperature as the main motions undergone by phenyl rings. These dynamical processes seem to be also

active in the blend components. As it has been shown for other polymeric mixtures, the local motions undergone in the glassy state are not appreciably affected by blending.[24]

At higher temperatures, an abrupt change in the slope of the effective mean squared displacement (see Fig. 2) is a signature of the glass-transition. We note that in the case of labelled samples like those here investigated, the calculation of the mean squared displacements is particularly subjected to uncertainties, due to coherent contaminations (see discussion in the SI). Therefore, to identify this transition we have directly calculated the temperature derivative of the measured elastic intensity function at 0.6 $Å^{-1}$, where the coherent contribution is low. Figure 13 shows the obtained results for the two blends investigated. This function shows always negative values –according to an increase of the mean squared displacement with increasing temperature. It displays a clear change in slope that reflects the start of the 'softening' of the component followed by the neutron scattering measurements. It occurs at about 220 K for hSBR in the hSBR/dPS blend and at about 240 K for hPS in the dSBR/hPS mixture. We can compare now these results with the distribution $g^c(T_{g,eff})$ for component c independently deduced from the above analysis of the BDS and QENS results. These functions are represented in Fig. 13 for the two components of the blends which are followed in the EFWS experiments. As can be appreciated, the kink in the EFWS derivative coincides with the temperatures at which $g^c(T_{g,eff})$ starts to present significant values. Thus, through its derivative, the elastic scans provide a microscopic probe to determine the onset of the effective glass-transition range of the labelled component in the blends.

On the other hand, regarding the comparison between dielectric and neutron scattering results, we note a significantly smaller value of $Q^\star$ for hPS than for hSBR. The meaning of the $Q^\star$ is not yet fully understood. In the case of a simple diffusive process, a simple approach based on molecular hydrodynamics and a molecular treatment of dielectric results allowed expressing $Q^\star$ in terms of a many body magnitude –a generalized Kirkwood parameter– and a single molecule magnitude –the hydrodynamic radius.[21,22] The generalization to the

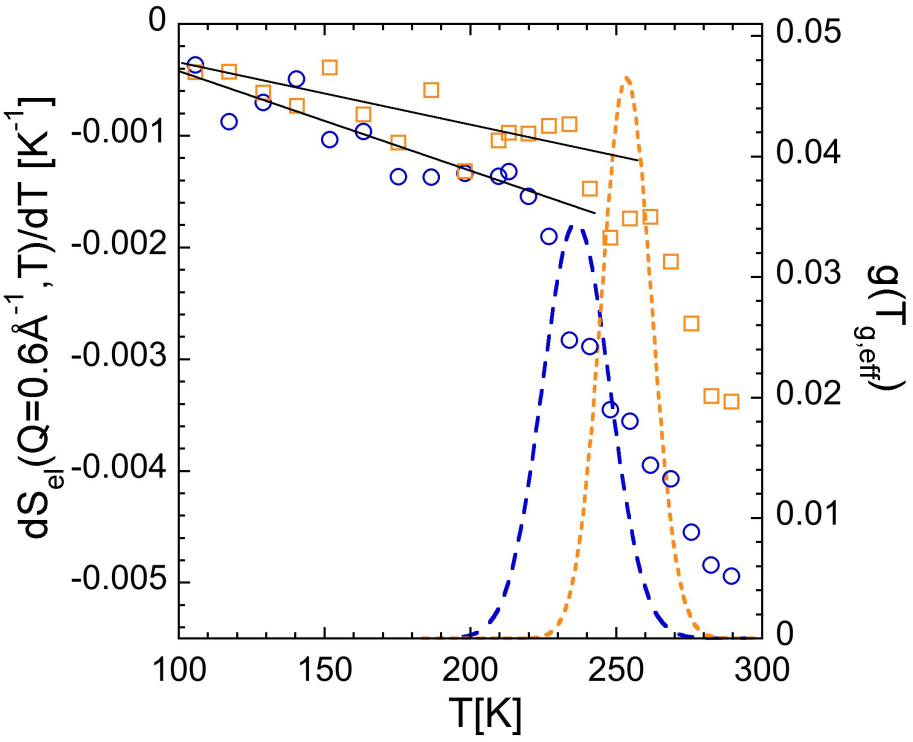

Figure 13: Derivative of $S_{el}(Q{=}0.6\ \text{Å}^{-1},T)$ with respect to temperature for the two blends investigated (circles: hSBR/dPS sample, squares: dSBR/hPS sample). The lines represent the deduced distributions of effective glass-transition temperatures for each of the components followed by the neutron scattering experiments.

case of polymeric materials showing anomalous diffusion is not straightforward, as recently shown.[37] A connection of $Q^\star$ with structural parameters like the position of the inter-main-chain correlation peak of the structure factor, Q_{max} was also explored in that work. Main-chain polymers (without side groups) or polymers with only methyl groups as side groups present rather similar values of $Q^\star \approx 0.9\ \mathring{A}^{-1}$ independently of the value of Q_{max}. However, for polymers with bulkier side groups, a correlation between $Q^\star$ and Q_{max} which is close to their equivalence $Q^\star = Q_{max}$ can be deduced, within the uncertainties. Actually, the case of PS fits in that framework. Moreover, some microscopic information can be inferred from a phenomenological analysis. Since applying the Gaussian approximation it can be deduced that $\langle r^2(t=\tau_{max}^{DS})\rangle = 6/Q^{\star 2}$,[21] the finding of a small value of $Q^\star$ suggests that atoms in PS need to reach large displacements to fully relax dipoles in the α-relaxation process.

We finally consider the information provided by the QENS experiments on both the

stretching and deviations from Gaussian behavior of the incoherent scattering function of the protons of the polymers. In principle, it could be expected that the presence of concentration fluctuations in the blend would give rise to more stretched functional forms and stronger deviations from Gaussian behavior than in the corresponding homopolymers, and that these effects would become more pronounced with decreasing temperature. As shown in Figs. 5 and 6, for a given temperature the effect of blending on SBR is to amplify the stretching. However, no significant impact on the Gaussian behavior is found, within the experimental uncertainties. For PS, at the temperature where data on the homopolymer have been recorded, we observe that both, stretching and non-Gaussian effects, become weaker upon blending with SBR (Figs. 6 and 7), contrarily to the a priori expectations. As previously pointed out, for a given temperature the PS component in the blend shows more pronounced stretching and non-Gaussian effects than the SBR component; also, its characteristic time is markedly longer.

Stretching and non-Gaussian effects following from heterogeneities tend to become weaker with increasing temperature due to the homogeneization of the molecular motions of the system with increasingly fast associated characteristic times. This is expected to happen already in homopolymers, and in fact it is the case here reported for hSBR, for which QENS data are available at different temperatures (Figs. 5 and 6). The faster the motions, the narrower becomes the distribution of characteristic times and consequently the closer to Gaussian is the probability distribution function of atomic displacements. Therefore, a suitable parameter to characterize the state of the system and compare different situations for different samples is using the characteristic time (isochronal representation). In Fig. 14 we have used as key variable the QENS relaxation time at a representative Q-value, namely $Q^{\star}$, to compare the stretching and non-Gaussian effects of the protons in the different components and/or conditions. In this representation, we observe that the behavior is practically independent of the particular environment and temperature of the sample. For a given value of $\tau(Q^{\star})$, all data show similar values, within the uncertainties, for both β and $\beta \cdot b$ parameters.

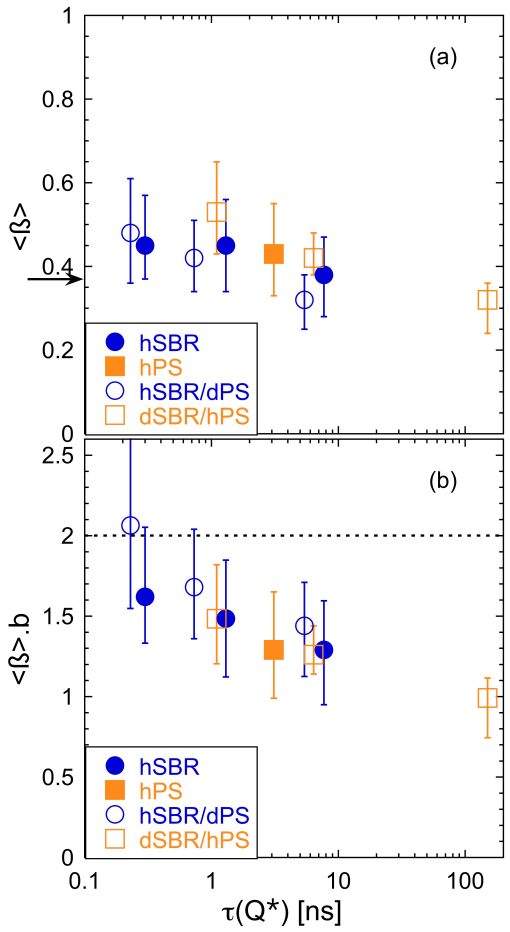

Figure 14: Data shown in Fig. 6 are represented here as function of the characteristic time at $Q^{\star}$.

The reason for these observations could be the intrinsic particularly marked heterogeneous and non-Gaussian behavior of the PS and SBR homopolymers. QENS is sensitive to atomic (protonic) motions, which are expected to be rather different for the diverse hydrogens located either at the phenyl rings or at the main chains. The Q-dependence of the stretching parameter and the large deviations from Gaussian behavior found for both homopolymers could be signatures of such heterogeneous microscopic motions. Being a random copolymer, we note that for SBR the situation is even more dramatic: also at the backbone, a highly heterogeneous dynamics is expected to take place since the atoms in the butadiene units

would present an enhanced mobility with respect to the main-chain styrene atoms. In the high-temperature range investigated by QENS, the distributions of mobilities induced by concentration fluctuations in the blends $G(\log\tau) = h(T_0)\frac{dT_0}{d\log(\tau)}$ are expected to be relatively narrow (see SI). Therefore, the main effect of blending at such high temperatures is to modify the overall timescale of the molecular motions, and the observed stretching and non-Gaussian behavior obey primarily to those intrinsically present in the homopolymers in an isochronal situation.

We note that in the analysis of experimental QENS results on polymers, the stretching of the α-relaxation contribution is usually assumed to be Q-independent. Some molecular dynamics (MD) simulations results have explored its possible variation with Q, in particular in the framework of the applicability of the Mode Coupling Theory (MCT). It is found that there is a tendency of the β-value to decrease with increasing Q, reaching asymptotic values of 0.24 (polybutadiene, PB)[4] or 0.35 (poly(vinyl methyl ether), PVME)[38] at high Qs. In the Q-range here investigated, the Q-variation of the β-values of the polymers (both, in the homopolymer and in the blend samples) is stronger than those found from MD-simulations in the above commented works. High-Q asymptotic β values even smaller than those reported for PB and PVME would be expected for SBR and PS, underlining the role of the dynamic arising from their complex microstructures.

Conclusions

In this work we have shown that the concepts and methodologies developed for the investigation of blend dynamics in systems composed of relatively simple homopolymers can be transferred to other more complex mixtures, particularly to a simplified industrial system involving the mixture of a random copolymer, SBR, with an oligomer, PS. The main conceptual ingredients are dynamic heterogeneity and concentration fluctuations, and the methodology involves the combination of different experimental techniques including DSC, BDS and

QENS. As a part of this methodology, the investigation by neutron scattering techniques of isotopically labelled samples was a requirement in order to isolate the response of one of the components in the mixture. This yield to face the problem of comparing results from samples which are not exactly equivalent. We have shown that thanks to the combination of neutron scattering techniques (sensitive to the isotopic details) with dielectric relaxation data (where the isotopic labeling should not play a role) covering a broad frequency range, a complete description of the segmental dynamics *of the two* polymer components in a complex mixture was possible. In this way, we resolved the fragility of the two components in the blend and identified the distribution of effective glass-transition temperatures of each blend component that nicely match the whole glass-transition range of the mixture as determined by DSC. The agreement is also good for each individual component when the distribution of effective glass-transition temperatures is compared with the corresponding EFWS neutron scattering results. This suggests the possibility of using EFWS as a direct way to determine the onset of the effective glass transition of the components of a mixture.

Finally, since in the high-temperature range accessed by QENS the distributions of mobilities induced by concentration fluctuations are expected to be narrow, the observed stretching and non-Gaussian behavior of the scattering function can be attributed to the intrinsically heterogeneous microscopic motions occurring in these relatively complex polymeric chains. The characterization of concentration fluctuations in these systems can be carried out by small angle neutron scattering experiments. These measurements are being performed and their connection with the dynamic response will be discussed in a future publication.

Acknowledgement

We thank Robert Ngo for SBR synthesis and Drs. M. Zamponi and M. Khaneft for their assistance in the SPHERES experiments. The authors gratefully acknowledge the financial support of the Basque Government code: IT-654-13 and the Ministerio de Economía y

Competitividad code: MAT2015-63704-P (MINECO/FEDER, UE). This work is based on experiments performed at DNS[39,40] operated at Jülich Centre for Neutron Science (JCNS), TOFTOF,[41] operated by the Technische Universität München, and SPHERES (Heinz Maier-Leibnitz Zentrum (MLZ), Garching, Germany), and has been supported by the European Commission under the 7th Framework Programme through the 'Research Infrastructures' action of the 'Capacities' Programme, NMI3-II Grant Number 283883.

Supporting Information Available

The Supporting Information presents: (i) the results obtained by diffraction with polarization analysis; (ii) the calculation of the effective mean squared displacements of the hydrogens of the protonated components in the blends from the elastic fixed window scan results; (iii) an estimation of the diffusive component in the oligomer (iv) the relationship between the frequency domain and the time domain relaxation function, and how to transform a KWW characteristic time into the maximum of the corresponding susceptibility; (v) the effects of the different microstructures of the protonated homopolymers and their deuterated counterparts on the dielectric signal; (vi) the comparison of characteristic times obtained by QENS for the two components in the blends; (vii) the determination of the value of $Q^{\star}$ from the comparison of the characteristic times obtained by quasielastic neutron scattering at different Q-values and by dielectric spectroscopy for the hSBR sample; (viii) the distribution functions of relaxation times deduced from the applied model.

References

(1) Utracki, L., Wilkie, C., Eds. *Polymer Blends Handbook*; Springer Netherlands, 2014.

(2) Ward, I. M.; Sweeney, J. *Mechanical Properties of Solid Polymers*; John Wiley and Sons, Ltd, 2013.

(3) Isayev, A. I., Ed. *Encyclopedia of Polymer Blends, Volume 1: Fundamentals*; Wiley, 2010.

(4) Colmenero, J.; Arbe, A. Segmental Dynamics in Miscible Polymer Blends: Recent Results and Open Questions. *Soft Matter* **2007**, *3*, 1474–1485.

(5) Chung, G. C.; Kornfield, J. A.; Smith, S. D. Component Dynamics Miscible Polymer Blends: A Two-Dimensional Deuteron NMR Investigation. *Macromolecules* **1994**, *27*, 964–973.

(6) Arbe, A.; Alegría, A.; Colmenero, J.; Hoffmann, S.; Willner, L.; Richter, D. Segmental Dynamics in Poly(vinylethylene)/Polyisoprene Miscible Blends Revisited. A Neutron Scattering and Broad-Band Dielectric Spectroscopy Investigation. *Macromolecules* **1999**, *32*, 7572–7581.

(7) Alegría, A.; Colmenero, J.; Ngai, K. L.; Roland, C. M. Observation of the Component Dynamics in a Miscible Polymer Blend by Dielectric and Mechanical Spectroscopies. *Macromolecules* **1994**, *27*, 4486–4492.

(8) Lodge, T. P.; Wood, E. R.; Haley, J. C. Two Calorimetric Glass Transitions Do Not Necessarily Indicate Immiscibility: The Case of PEO/PMMA. *Journal of Polymer Science Part B: Polymer Physics* **2006**, *44*, 756–763.

(9) Shenogin, S.; Kant, R.; Colby, R. H.; Kumar, S. K. Dynamics of Miscible Polymer Blends: Predicting the Dielectric Response. *Macromolecules* **2007**, *40*, 5767–5775.

(10) Lodge, T. P.; McLeish, T. C. B. Self-Concentrations and Effective Glass Transition Temperatures in Polymer Blends. *Macromolecules* **2000**, *33*, 5278–5284.

(11) Cangialosi, D.; Alegría, A.; Colmenero, J. "Self-concentration" Effects on the Dynamics of a Polychlorinated Biphenyl Diluted in 1,4-Polybutadiene. *The Journal of Chemical Physics* **2007**, *126*.

(12) Kahlau, R.; Bock, D.; Schmidtke, B.; Rössler, E. Dynamics of Asymmetric Binary Glass Formers. I. A Dielectric and Nuclear Magnetic Resonance Spectroscopy Study. *The Journal of Chemical Physics* **2014**, *140*, 044509.

(13) Kremer, A., Friedrich; Schönhals, Ed. *Broadband Dielectric Spectroscopy*; Springer, 2003.

(14) Sakai, V. G.; Arbe, A. Quasielastic Neutron Scattering in Soft Matter. *Current Opinion in Colloid & Interface Science* **2009**, *14*, 381–390.

(15) Guillermo, A.; Lartigue, C.; Cohen Addad, J. P. PEO Temporary Network in PEO/PMMA Blends: NMR Approach. *Macromolecules* **1998**, *31*, 769–775.

(16) Arbe, A.; Colmenero, J.; Richter, D. Polymer Dynamics by Dielectric Spectroscopy and Neutron Scattering. *Broadband Dielectric Spectroscopy Chap. 18, Springer* **2003**,

(17) Bouty, A.; Petitjean, L.; Chatard, J.; Matmour, R.; Degrandcourt, C.; Schweins, R.; Meneau, F.; Kwasniewski, P.; Boue, F.; Couty, M.; Jestin, J. Interplay between polymer chain conformation and nanoparticle assembly in model industrial silica/rubber nanocomposites. *Faraday Discuss.* **2016**, *186*, 325–343.

(18) Scharpf, O.; Capellmann, H. *Phys. Status Solidi A* **1993**, *A27*, 359.

(19) Williams, G.; Watts, D. C. Non-symmetrical dielectric relaxation behaviour arising from a simple empirical decay function. *Transactions of the Faraday Society* **1970**, *66*, 80–85.

(20) Richter, D.; Monkenbusch, M.; Arbe, A.; Colmenero, J. *Neutron Spin Echo in Polymer Systems*; Adv. Polym. Sci.; Springer Verlag, Berlin Heidelberg New York, 2005; Vol. 174.

(21) Arbe, A.; Malo de Molina, P.; Alvarez, F.; Frick, B.; Colmenero, J. Dielectric Susceptibility of Liquid Water: Microscopic Insights from Coherent and Incoherent Neutron Scattering. *Physical Review Letters* **2016**, *117*, 185501.

(22) Malo de Molina, P.; Alvarez, F.; Frick, B.; Wildes, A.; Arbe, A.; Colmenero, J. Investigation of the Dynamics of Aqueous Proline Solutions Using Neutron Scattering and Molecular Dynamics Simulations. *Physical Chemistry Chemical Physics* **2017**, *19*, 27739–27754.

(23) Tyagi, M.; Alegría, A.; Colmenero, J. Heterogeneous Dynamics of Poly(vinyl acetate) Far Above Tg: A Combined Study by Dielectric Spectroscopy and Quasielastic Neutron Scattering. *The Journal of Chemical Physics* **2005**, *122*.

(24) Cendoya, I.; Alegría, A.; Alberdi, J. M.; Colmenero, J.; Grimm, H.; Richter, D.; Frick, B. Effect of Blending on the PVME Dynamics. A Dielectric, NMR, and QENS Investigation. *Macromolecules* **1999**, *32*, 4065–4078.

(25) Vogel, H. The Law of the Relationship Between Viscosity of Liquids and the Temperature. *Physikalische Zeitschrift* **1921**, *22*, 645–646.

(26) Fulcher, G. S. Analysis of Recent Measurements of the Viscosity of Glasses. *Journal of the American Ceramic Society* **1925**, *8*, 339–355.

(27) Tammann, G.; Hesse, W. Die Abhängigkeit der Viscosität von der Temperatur bei unterkühlten Flüssigkeiten. *Zeitschrift für anorganische und allgemeine Chemie* **1926**, *156*, 245–257.

(28) Arbe, A.; Richter, D.; Colmenero, J.; Farago, B. Merging of the α and β Relaxations in Polybutadiene: A Neutron Spin Echo and Dielectric Study. *Physical Review E* **1996**, *54*, 3853–3869.

(29) Narros, A.; Arbe, A.; Alvarez, F.; Colmenero, J.; Richter, D. Atomic Motions in the $\alpha\beta$-Merging Region of 1,4-Polybutadiene: A Molecular Dynamics Simulation Study. *The Journal of Chemical Physics* **2008**, *128*, 224905.

(30) Alvarez, F.; Alegría, A.; Colmenero, J. Interconnection Between Frequency-Domain Havriliak-Negami and Time-Domain Kohlrausch-Williams-Watts Relaxation Functions. *Physical Review B* **1993**, *47*, 125–130.

(31) Kumar, S. K.; Shenogin, S.; Colby, R. H. Dynamics of Miscible Polymer Blends: Role of Concentration Fluctuations on Characteristic Segmental Relaxation Times. *Macromolecules* **2007**, *40*, 5759–5766.

(32) Arrese-Igor, S.; Alegría, A.; Moreno, A. J.; Colmenero, J. Effect of Blending on the Chain Dynamics of the "Low-Tg"Component in Nonentangled and Dynamically Asymmetric Polymer Blends. *Macromolecules* **2011**, *44*, 3611–3621.

(33) Goracci, G.; Arbe, A.; Alegría, A.; Su, Y.; Gasser, U.; Colmenero, J. Structure and Component Dynamics in Binary Mixtures of Poly(2-(dimethylamino)ethyl methacrylate) with Water and Tetrahydrofuran: A Diffraction, Calorimetric, and Dielectric Spectroscopy Study. *The Journal of Chemical Physics* **2016**, *144*.

(34) Angell, C. A. Perspective on the Glass Transition. *Journal of Physics and Chemistry of Solids* **1988**, *49*, 863–871.

(35) Saiter, J. M.; Grenet, J.; Dargent, E.; Saiter, A.; Delbreilh, L. Glass Transition Temperature and Value of the Relaxation Time at Tg in Vitreous Polymers. *Macromolecular Symposia* **2007**, *258*, 152–161.

(36) Arrese-Igor, S.; Arbe, A.; Frick, B.; Colmenero, J. Glassy Dynamics of Polystyrene by Quasielastic Neutron Scattering. *Macromolecules* **2011**, *44*, 3161–3168.

(37) Arbe, A.; Colmenero, J. Relaxation Processes in Liquids and Glass-Forming Systems: What Can We Learn by Comparing Neutron Scattering and Dielectric Spectroscopy Results? *Kremer, F. Loidl, A. (Eds.) Springer, 2018.*

(38) Capponi, S.; Arbe, A.; Alvarez, F.; Colmenero, J.; Frick, B.; Embs, J. P. Atomic Motions in Poly(vinyl methyl ether): A Combined Study by Quasielastic Neutron Scattering and Molecular Dynamics Simulations in the Light of the Mode Coupling Theory. *The Journal of Chemical Physics* **2009**, *131*.

(39) Su, Y.; Nemkovski, K. *Journal of large-scale research facilities.* **2015**, *A27*, 376–388.

(40) Schweika, W.; Boni, P. *Physica B* **2001**, *A27*, 155.

(41) Heinz-Maier-Leibnitz-Zentrum., Cold Neutron Time-of-Flight Spectrometer. *Journal of large-scale research facilities.*

Graphical TOC Entry